# DESIGN AND EXPERIMENTAL EVALUATION OF A DIRECT-INJECTION WINGED SHOVEL FOR A DEEP STRAW INCORPORATION MACHINE

/

# 秸秆深埋还田机直注翼铲设计与试验评价

**Sicheng YANG[1], Lihua WEI*[1], Fanbowen MENG[1], Deshuai LI[1], Jiantian LI[2], Zhengqing WANG[1],Ruili WANG*[1]**

[1]College of Engineering, Shenyang Agricultural University, Shenyang / China;

[2]Fengcheng Caohe Machinery Manufacturing Co., Ltd., Dandong / China.

*Corresponding authors. Lihua Wei; Tel: +86 13386825657; E-mail: weilihua@syau.edu.cn;*

*Ruili Wang, Tel: +86 17702424189; E-mail: wangruili@syau.edu.cn.*

*DOI: https://doi.org/10.35633/inmateh-79-61*

***Keywords:** straw deep burial machine, soil-direct-injection wing shovel interaction, Box-Behnken design, soil coverage rate, response surface methodology*

## ABSTRACT

*Conventional deep-burial devices typically employ a split structure consisting of a furrowing shovel and a soil-covering plate. During field operation, vibrations can cause relative displacement between these components, resulting in unstable soil coverage. Such devices may also exhibit structural redundancy, insufficient tillage depth, and high energy consumption. In this study, theoretical analysis and numerical simulation based on mechanical and soil-dynamics models were conducted to elucidate the soil–tool interaction mechanism of a direct-injection winged shovel and determine its key structural parameters. Using an EDEM-based soil–tool interaction model, a single-factor Box–Behnken experimental design was conducted with penetration angle, operating speed, and wing depth as the experimental factors and soil coverage rate and tillage resistance as the response variables. The optimal parameter combination consisted of a shovel-tip penetration angle of 25°, a wing depth of 150 mm, and an operating speed of 1.4 m·s⁻¹. Under these conditions, the direct-injection winged shovel achieved low tillage resistance, a high soil coverage rate, stable operation, and consistent furrow width. Field tests showed that all measured performance indicators met the requirements of the applicable Chinese national standards. The developed shovel exhibited stable and consistent performance during deep straw incorporation, thereby effectively improving operational quality.*

## 摘要

*传统深埋部件多采用开沟铲与覆土板分体装配结构，田间作业过程中易受振动发生相对偏移，造成覆土稳定性较差，同时存在结构冗余、耕深不足、作业能耗偏高等问题，为此本文创新设计一体化开沟覆土直注翼铲，单一部件可同步完成开沟、覆土、秸秆深埋、深松复合作业。采用理论分析与数值模拟相结合的方法，通过力学和土壤动力学分析模型，阐明直注翼铲与土壤的相互作用机制，确定直注翼铲主要结构参数。基于 EDEM 土壤耕作仿真模型，采用单因素试验 Box-Behnken 组合试验设计，以入土角、耕作速度、尾翼深度为试验因素，以覆土率、耕作阻力为核心评价指标，结果确定直注翼铲较优参数为铲尖入土角 25°、铲体尾翼深度 150 mm、耕作速度 1.4 m·s-1，该组参数下耕作阻力较小，自动覆土率高，作业稳定性与开沟宽度一致性较好。田间试验结构表明，该直注翼铲各项作业指标均符合国家标准要求，在秸秆还田作业中表现出良好的稳定性与一致性，能够有效提升作业质量。*

## INTRODUCTION

China is a major agricultural country with extremely abundant crop straw resources, accounting for nearly one-fifth of the global total (*Zhang et al., 2025*). Among them, the production of corn straw ranks first in the country, which is attributed to the continuous development of agricultural mechanization and has now become a necessary support condition for sustainable agricultural development (*Fang et al., 2021; Liu et al., 2025; Awachat et al., 2024; Wang et al., 2023)*. The deep straw incorporation machine buries postharvest crop residues in the subsoil, enabling their efficient incorporation at the required depth. The structural design and operational performance of its furrow-opening and soil-covering components directly affect the quality of straw burial *(Barr et al., 2020; Madhusudan et al., 2024)*.

Most straw incorporation machines currently available in China are designed only to pulverize and scatter straw or apply it as surface mulch, whereas only a limited number of models can incorporate crushed straw deep into the soil *(Shen et al., 2022)*.

This deep-burial device typically employs a split assembly structure comprising a furrowing shovel and a soil covering plate. Due to soil impact and machine vibration, component positions tend to deviate, leading to issues such as uneven soil coverage and insufficient backfilling. The separate connection components introduce structural redundancy, resulting in excessive tillage resistance for the entire unit. Current research lacks an integrated design capable of simultaneously performing furrowing, soil guidance, return flow, and directional soil covering, making it difficult to fundamentally address soil instability caused by positional deviations in the modular assembly (*Aikins et al., 2020*). In contrast, straw incorporation equipment developed in other countries offers greater automation and operational precision, together with compact designs and integrated functions. It can simultaneously perform multiple processes including straw pulverization, soil mixing, and deep burial, offering high operational efficiency and automation*(Lin et al., 2022; Xu et al., 2022)*. Such machine can adapt to various field cultivation needs. However, when applied domestically, these machines face challenges such as high costs, substantial maintenance expenses, and difficulty in adapting to local working conditions.

To address challenges in deep straw incorporation such as unstable soil coverage and high tillage resistance, this study developed a direct-injection wing shovel with the dual functions of furrowing and automatic soil covering, while optimizing its core structure and operational parameters. The effects of key structural parameters, including the penetration angle and tail-wing depth, on soil–tool interactions were analyzed. The physical and mechanical properties of the soil and the requirements for deep straw incorporation were then incorporated into a performance-optimization model. Based on theoretical analysis, an EDEM discrete element simulation was employed to construct a shovel-soil interaction model, identifying the optimal structural and operational parameter combination. Field trials were conducted to validate the shovel's operational efficiency.

## MATERIALS AND METHODS

### *Structure and Working Principle*

The deep straw incorporation machine shown in Fig. 1 consists of a three-point hitch frame, chain-drive system, main frame, soil-lifting and covering device, straw-crushing device, flow-guiding device, and transmission system. The machine is mounted on the rear three-point hitch of the tractor, and its transmission system is connected to the tractor power take-off (PTO) shaft through a universal joint *(Cedik et al., 2024)*. During operation, the shovel tip penetrates to a depth of 30 cm below the soil surface. Symmetrically arranged side blades driven by the chain-drive system further crush the preprocessed straw, reducing its particle size. The processed straw is conveyed by airflow through the fan outlet to the flow-guiding device, which collects it and directs it into the feeding tube. The tube then delivers the straw directly into the cavity created by the direct-injection winged shovel as it lifts and displaces the soil. The displaced soil subsequently falls back automatically, covering the accumulated straw at a depth of approximately 30 cm within the subsoil layer. This process enables the concentrated placement and deep incorporation of straw. By promoting straw decomposition and increasing the organic matter returned to the soil, this method can improve soil structure and create favorable conditions for subsequent crop growth.

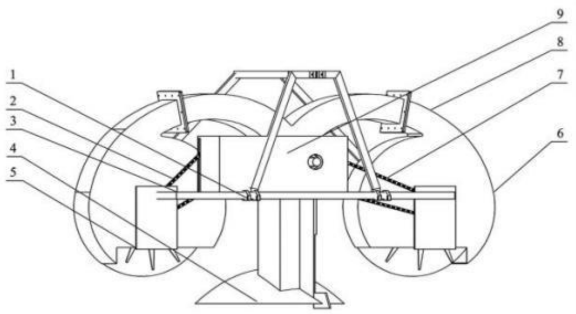


**Fig. 1 - Structural schematic of the deep straw incorporation machine**

*1. Three-point hitch frame; 2. Left chain-drive system; 3. Main frame; 4. Soil-lifting and covering device; 5. Straw-crushing device; 6. Fan housing; 7. Right chain-drive system; 8. Flow-guiding device; 9. Transmission system.*

***Design of the direct-injection winged shovel for furrow opening and soil covering***

The direct-injection winged shovel shown in Fig. 2 consists of a shovel body, feeding tube, support plate, and soil-guiding rails.

The device delivers crushed straw beneath the cultivated soil layer, while its structural configuration promotes the automatic return of displaced soil, thereby ensuring uniform straw burial and restoration of the soil profile. During operation, the wing-shaped shovel body lifts and displaces the soil, forming a subsurface cavity for deep straw placement. The coordinated design of the feeding tube and shovel body allows the crushed straw to pass smoothly into this cavity. As the shovel advances, the displaced soil falls back over the deposited straw, ensuring deep burial while maintaining a relatively level soil surface and a stable soil profile. The shovel also disrupts the compacted layer beneath the cultivated soil, increasing soil porosity and potentially improving soil aeration, water infiltration, and root development.

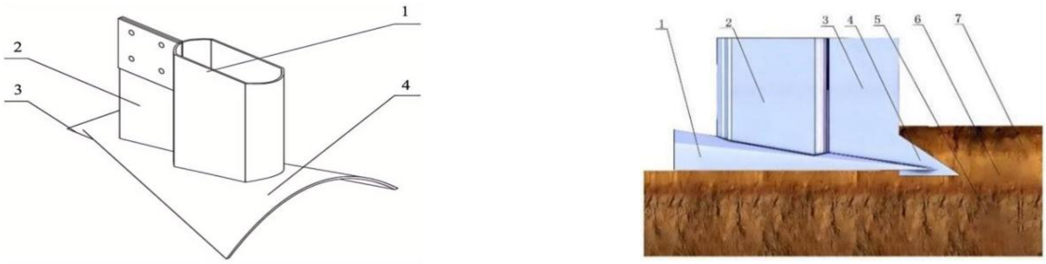


**Fig. 2 - Structural schematic of the direct-injection winged shovel and its position within the soil profile**

*1. feeding tube; 2. shovel body; 3. support plate; 4. soil-guiding rail; 5. tillage layer; 6. plough pan; 7. subsoil*

Analysis of the Operating Process

The following assumptions were adopted to establish the analytical model: (1) the shovel moves forward at a constant velocity, and acceleration during startup and stopping is neglected; (2) the soil is regarded as a homogeneous elastoplastic medium; (3) stones, crop residues, and other randomly distributed inclusions are excluded; and (4) only the soil stress state under steady-state cutting conditions is considered. Figure 3 illustrates the forces acting on the soil during operation of the direct-injection winged shovel. The soil–tool interaction process is divided into three regions: AB, BC, and BD. In region AB, the soil is primarily subjected to its weight $G_1$, the friction force $f$ generated by relative motion along the contact surface, and the normal force $F_1$ exerted by the shovel tip. The weight $G_1$ acts vertically downward, $f$ acts tangentially to the upper surface of the shovel tip, and $F_1$ exerted by the shovel tip acts perpendicular to the shovel-tip surface. In region BC, the support plate acts on the soil, which is subjected to its weight $G_2$ and the contact force $F_2$ exerted by the plate. This interaction compresses, shears, and fractures the soil, resulting in structural deformation. In region BD, the shovel body interacts with the soil, which is subjected to its weight $G_3$, the normal force $F_3$ exerted by the side surface of the shovel body, and the longitudinal compressive force $F_4$, acting in the direction of travel.

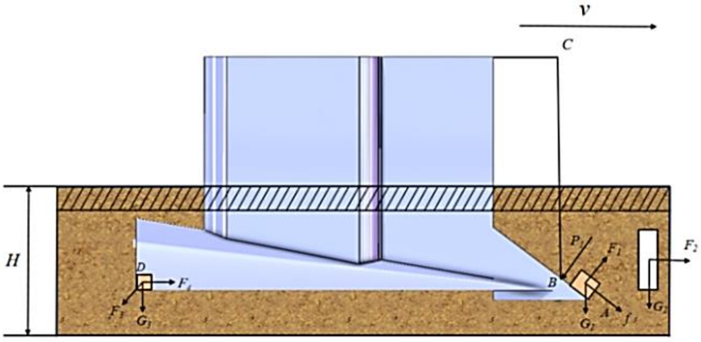


**Fig. 3 - Diagram of soil forces**

Force analysis during the earth-breaking process

During operation of the direct injection wing shovel, the wedge-shaped soil mass formed ahead of its working area is lifted and subsequently fragmented, preventing soil overturning. As the shovel advances, its blade continuously cuts through the soil while encountering horizontal tillage resistance. The combined traction resistance $P$ generated by the blade tip and handle during soil cutting is calculated as:

$$P = k_1 l_1 + k_2 l_2 \tag{1}$$

In the formula: $k_1$ and $k_2$ represent the components of resistance in the direction of movement per unit length; $l_1$ and $l_2$ denote the lengths of the blade tip and handle blade, respectively (mm).

Analysis of Soil cutting failure motion

During cultivation, the shovel blades compress the soil, causing shear damage. The horizontal component of the force acting on the shovel blades is the traction resistance $T$:

$$T = N\sin\alpha + F\cos\alpha = N(\sin\alpha + f\cos\alpha) \tag{2}$$

where $N$ is the normal pressure, $F$ is the friction force of the soil on the shovel tip, and $\theta$ is the penetration angle of the direct-injection winged shovel.

The normal stress level of soil is the correlation coefficient of soil. Assuming that the working area of the straight injection wing shovel is $A$, then the normal pressure $N$ is:

$$N = A \cdot \xi \cdot \delta\Delta t \tag{3}$$

Furthermore:

$$f = tan\,\phi \tag{4}$$

where $\varphi$ denotes the soil's friction angle.

The traction resistance $T$ is given by:

$$T = A \cdot \xi \cdot \delta(sin\,\alpha + f\,cos\,\alpha) = A \cdot \xi \cdot \delta(sin\,\alpha + tan\,\phi\,cos\,\alpha) \tag{5}$$

This set of mechanical equations establishes the theoretical relationship among the penetration angle, contact area, and traction resistance, thereby determining the appropriate range for the penetration angle and providing a theoretical basis for selecting factor levels in subsequent Box-Behnken experiments, while establishing an intrinsic connection between the theoretical model and the experimental design.

**Structural Optimization**

Single-factor experiment

As shown in Figure 4(a), when the penetration angle of the direct-injection wing shovel falls within the range of 19-28°, the soil coverage rate decreases gradually with increasing penetration angle; whereas within the range of 28-32°, the coverage rate exhibits a negative correlation with the penetration angle. Figure 4(b) demonstrates that for penetration angles between 19° and 25°, tillage resistance increases steadily and slowly with increasing angle, while for angles between 25° and 32°, tillage resistance shows an inverse relationship with the penetration angle. Considering the optimization of both soil coverage rate and tillage resistance, an optimal penetration angle range of 22-25° is identified as achieving both significantly improved soil coverage efficiency and effective reduction of tillage resistance.

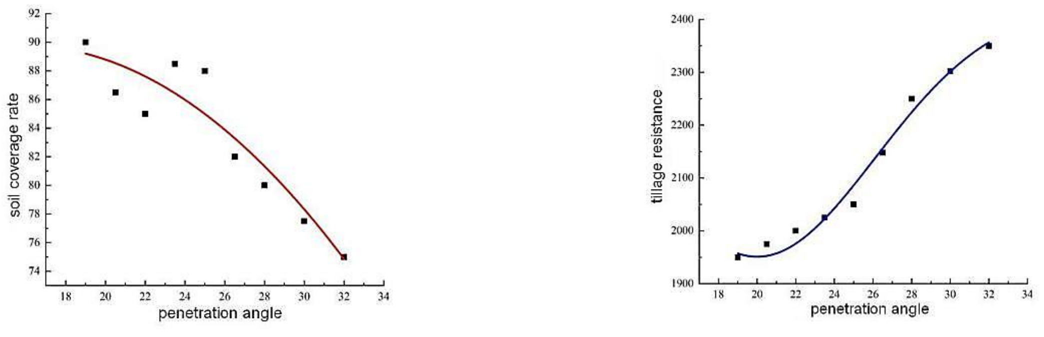


*(a) Soil coverage rate at different penetration angles* *(b) Tillage resistance at different penetration angles*

**Fig. 4 - Effects of shovel tip penetration angle on test indicators**

As the depth of the plow body tail wing increases, the soil coverage rate remains generally stable; however, a turning point occurs at a tail wing depth of 150 mm, where the decline rate accelerates significantly. An optimal tail wing depth helps reduce tillage resistance and lower operational energy consumption. Considering the combined effects of tail wing depth on both soil coverage rate and tillage resistance, an ideal range of 120-150 mm is identified, which yields high soil coverage while minimizing tillage resistance.

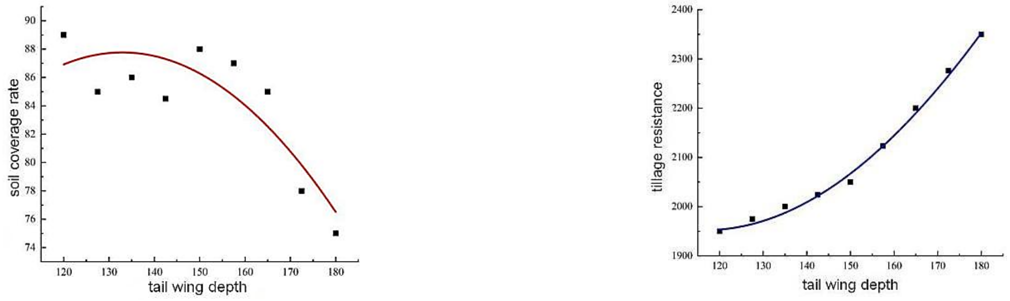


*(a) Soil coverage rate at different tail wing depths* *(b) Tillage resistance at different tail wing depths*

**Fig. 5 - Effects of shovel body tail wing depth on test indicators**

The effects of different tillage speeds on soil coverage rate and tillage resistance are illustrated in Figure 6. The experimental results demonstrate that tillage speed significantly influences both coverage rate and tillage resistance. The coverage rate generally decreases with increasing tillage speed, whereas the trend for tillage resistance is opposite. This relationship remains stable within the speed range of 1.2-1.6 m/s. Within this range, an optimal tillage speed can be identified—one that maintains adequate soil coverage by the direct-injection wing shovel while effectively reducing tillage resistance.


*(a) Soil coverage rate at different tillage speeds* *(b) Tillage resistance at different tillage speeds*

**Fig. 6 - Effects of tillage speed on test indicators**

Establishment of the simulation model

The direct-injection winged shovel consists of a shovel body, feeding tube, support plate, and soil-guiding rail, as shown in Fig. 3. A 3D model of the shovel was developed in SolidWorks, exported in IGS format, and imported into EDEM. The material properties, contact parameters, and mechanical parameters required for the discrete element method (DEM) simulation were then defined. The parameters used in the simulation are presented in Table 1.

**Table 1**

| Parameter | Numeric value |
|---|---|
| Poisson's ratio of the direct-injection winged shovel (45 steel) | 0.25 |
| Shear modulus of the direct-injection winged shovel (45 steel) (Pa) | $8.21\times10^{10}$ |
| Density of the direct-injection winged shovel (45 steel) (kg·m$^{-3}$) | 7900 |
| Shear modulus of the cultivated-layer soil (Pa) | $1\times10^{6}$ |
| Density of the cultivated-layer soil (kg·m$^{-3}$) | 1440 |
| Bond stiffness of the cultivated-layer soil (km·m$^{-3}$) | $5\times10^{7}$ |
| Bond strength of the cultivated-layer soil (Pa) | $2\times10^{4}$ |
| Coefficient of friction of the cultivated-layer soil | 0.333 |
| Poisson's ratio of the plow-pan soil | 0.36 |
| Shear modulus of the plow-pan soil (Pa) | $1.1\times10^{6}$ |
| Density of the plow-pan soil (kg·m$^{-3}$) | 1500 |
| Bond stiffness of the plow-pan soil (km·m$^{-3}$) | $5\times10^{7}$ |
| Bond strength of the plow-pan soil (Pa) | $3\times10^{4}$ |
| Coefficient of friction of the plow-pan soil | 0.282 |
| Poisson's ratio of the subsoil | 0.36 |
| Shear modulus of the subsoil (Pa) | $1.2\times10^{6}$ |
| Density of the subsoil (kg·m$^{-3}$) | 1540 |
| Bond stiffness of the subsoil (km·m$^{-3}$) | $5\times10^{7}$ |
| Bond strength of the subsoil (Pa) | $4\times10^{4}$ |
| Coefficient of friction of the subsoil | 0.224 |

The contact model is a fundamental component of the discrete element method (DEM), as it describes the forces and deformations generated by particle–particle and particle–boundary interactions *(Liu et al., 2025)*. Commonly used contact models include Hertz–Mindlin with JKR, the Parallel Bond Model, and Hertz–Mindlin with Bonding. The Hertz–Mindlin with JKR model accounts for adhesive forces at particle contacts but does not explicitly represent the fracture of cemented bonds. The Parallel Bond Model is widely used to simulate the fracture of brittle bonded materials, such as rock, but may require extensive calibration for soil applications. Considering both simulation accuracy and computational efficiency, the Hertz–Mindlin with Bonding model was selected in this study.

By allowing bonds between particles to break when prescribed strength criteria are exceeded, this model can represent soil cracking, shear failure, and the separation and movement of soil layers during tillage. It was therefore considered suitable for simulating the interaction between the direct-injection winged shovel and the soil.

The soil in this experimental area is sandy loam, with the plow pan extending from the surface to a depth of 150 mm. Soil physical analysis reveals that this layer exhibits high porosity and soft texture, primarily composed of granular and columnar soil particles. Below 150 mm lies the shovel subsoil, which shows significantly increased compaction and greater hardness, with soil particles consisting of individual grains and clumps. The core soil layer below 300 mm is classified as the non-plow pan, mainly composed of large-sized kernel-like particles.

For numerical simulations of deep loosening operations, a scaled virtual soil tank was developed with dimensions of 2000 mm × 1200 mm × 450 mm, designed to mitigate boundary effects. Soil parameters were stratified across three layers: 0–150 mm, 150–300 mm, and 300–450 mm, corresponding to the tillage, shovel, and core soil layers, respectively *(Wei et al., 2025)*. A discretized soil particle model was then constructed to balance computational efficiency and the representation of soil structural characteristics, as presented in Fig.7.

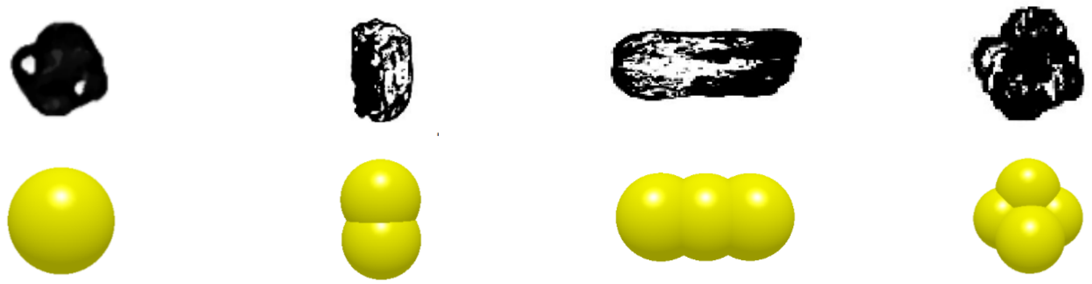


**Fig. 7 - Soil particle model**

Simulation test analysis

Based on the parameter ranges determined through preliminary single-factor experiments, a Box–Behnken experimental design was developed using Design-Expert 13. The experimental factors and their coded levels are presented in Table 2.

**Table 2**

**Table of factor level coding**

| Level | Factor | | |
|---|---|---|---|
| | Penetration angle *A* / (°) | Tail wing depth *B* / mm | Tillage speed *C* / (m·s$^{-1}$) |
| -1 | 22 | 135 | 1.2 |
| 0 | 25 | 150 | 1.4 |
| 1 | 28 | 165 | 1.6 |

## RESULTS

### *Analysis of variance of the simulation results*

A Box–Behnken experimental design was developed using Design-Expert 13, and the simulations were performed according to the resulting design matrix. The design comprised 17 runs, including five replicates at the center point, to estimate experimental error and assess model adequacy. The objective was to determine the effects of three factors—the penetration angle (A), tail-wing depth (B), and operating speed (C)—on the soil coverage rate and tillage resistance of the direct-injection winged shovel. The design matrix and simulation results are presented in Table 3.

Table 3

**Experimental design and simulation results**

| Run | Penetration angle A / [°] | Tail wing depth B / [mm] | Tillage speed C / [min] | Soil coverage rate $Y_1$ / [%] | Tillage resistance $Y_2$ / [N] |
|---|---|---|---|---|---|
| 1 | 25 | 150 | 1.4 | 88.79 | 2060.33 |
| 2 | 22 | 150 | 1.6 | 82.43 | 2073.33 |
| 3 | 25 | 165 | 1.2 | 79.83 | 2065.09 |
| 4 | 25 | 135 | 1.6 | 79.23 | 2282.48 |
| 5 | 22 | 135 | 1.4 | 79.70 | 2233.33 |
| 6 | 28 | 135 | 1.4 | 77.43 | 2370.38 |
| 7 | 28 | 165 | 1.4 | 80.43 | 2160.92 |
| 8 | 28 | 150 | 1.2 | 79.77 | 2153.73 |
| 9 | 25 | 150 | 1.4 | 87.99 | 2055.33 |
| 10 | 25 | 165 | 1.6 | 82.23 | 2162.54 |
| 11 | 25 | 150 | 1.4 | 88.23 | 2051.33 |
| 12 | 22 | 165 | 1.4 | 81.70 | 2083.33 |
| 13 | 28 | 150 | 1.6 | 78.17 | 2280.69 |
| 14 | 25 | 135 | 1.2 | 78.83 | 2295.91 |
| 15 | 25 | 150 | 1.4 | 88.03 | 2049.33 |
| 16 | 22 | 150 | 1.2 | 80.03 | 2136.33 |
| 17 | 25 | 150 | 1.4 | 88.43 | 2099.33 |

Significance analysis of soil coverage rate $Y_1$ and tillage resistance $Y_2$ with direct injection wing shovel

A variance analysis and regression coefficient significance test were performed on the regression model of soil coverage rate $Y_1$ for direct injection wing shovels, with detailed results presented in Table 4. The regression equation for soil coverage rate $Y_1$ is as follows:

$$\hat{Y}_1 = 88.29\text{-}1.01A + 1.12B + 0.45C + 0.25AB - AC + 0.5BC - 4.2A^2 - 4.27B^2 - 3.99C^2 \tag{5}$$

A model is considered significant when its F-value reaches 177.94. In this context, a P-value below 0.0500 indicates a statistically significant model term, while a P-value below 0.01 signifies extremely significant. The specific P-values are: A (0.0002), B (0.0001), C (0.0172), AC (0.0018), BC (0.0448), $A^2$ (0.0001), and $B^2$ (0.0001). Therefore, terms A, B, C, AC, $A^2$, $B^2$, and $C^2$ are all statistically significant. The out-of-fit term shows an F-value of 2.3 with a P-value of 0.2189, indicating that the out-of-fit term is not significant. This suggests the model fits well and the data is reliable.

Table 4

**Analysis of variance of coverage rate**

| Source of variation | Sum of square | Degree of freedom | Mean square | F value | P value | Significance |
|---|---|---|---|---|---|---|
| Model | 269.20 | 9 | 29.91 | 177.94 | < 0.000 1 | ** |
| A | 8.12 | 1 | 8.12 | 48.31 | 0.0002 | ** |
| *B* | 10.12 | 1 | 10.12 | 60.23 | 0.0001 | ** |
| *C* | 1.62 | 1 | 1.62 | 9.64 | 0.0172 | * |
| AB | 0.2500 | 1 | 0.2500 | 1.49 | 0.2621 | |
| AC | 4.00 | 1 | 4.00 | 23.80 | 0.0018 | ** |
| *BC* | 1.0000 | 1 | 1.0000 | 5.95 | 0.0448 | * |
| $A^2$ | 74.44 | 1 | 74.44 | 442.87 | < 0.0001 | ** |
| $B^2$ | 76.94 | 1 | 76.94 | 457.73 | < 0.0001 | ** |
| $AB^2$ | 67.03 | 1 | 67.03 | 398.73 | < 0.0001 | ** |
| Residual | 1.18 | 7 | 0.1681 | | | |
| Lack of Fit | 0.7450 | 3 | 0.2483 | 2.30 | 0.2189 | |
| Pure Error | 0.4316 | 4 | 0.1079 | | | |
| Sum | 270.37 | 16 | | | | |

Note: $p \le 0.01$ means highly significant (**); $0.01 < p \le 0.05$ means significant (*); $p > 0.05$ means not significant.

The regression model for tillage resistance $Y_2$ of direct injection wing shovels was constructed. Through analysis of variance and regression coefficient significance test, the results are shown in Table 5. The regression equation for tillage resistance $Y_2$ is:

$$\hat{Y}_2 = 2063.13 + 54.93A - 88.78B + 18.5C - 14.87AB + 47.49AC + 27.72BC + 54.19A^2 + 94.67B^2 - 43.7C^2 \tag{6}$$

As shown in Table 5, A, B, and C represent the penetration angle, tail-wing depth, and operating speed, respectively, and tillage resistance is the response variable. The model F-value of 72.86 indicates statistical significance. A P-value below 0.0500 signifies a significant model term, while a P-value below 0.01 denotes extremely significant terms.

Specifically, the P-values for A and B are both <0.0001, C is 0.0135, AC is 0.1046, BC is 0.0103, $A^2$ is 0.0002, $B^2$ is <0.0001, and $C^2$ is 0.0008. Thus, A, B, C, AC, BC, $A^2$, $B^2$, and $C^2$ are significant model terms. The out-of-fit term has an F-value of 0.0566 and a P-value of 0.9799, indicating no significant out-of-fit term, suggesting good model fit and reliable data.

**Table 5**

**Analysis of variance of tillage resistance**

| Source of variation | Sum of square | Degree of freedom | Mean square | F value | P value | Significance |
|---|---|---|---|---|---|---|
| Model | $1.669\times10^5$ | 9 | 18540.22 | 72.86 | < 0.000 1 | ** |
| A | 24134.05 | 1 | 24134.05 | 94.84 | < 0.0001 | ** |
| *B* | 63051.56 | 1 | 63051.56 | 247.78 | < 0.000 1 | ** |
| *C* | 2737.26 | 1 | 2737.26 | 10.76 | 0.0135 | * |
| AB | 883.87 | 1 | 883.87 | 3.47 | 0.1046 | * |
| AC | 9021.20 | 1 | 9021.20 | 35.45 | 0.0006 | ** |
| *BC* | 3073.59 | 1 | 3073.59 | 12.08 | 0.0103 | * |
| $A^2$ | 12363.15 | 1 | 12363.15 | 48.58 | 0.0002 | ** |
| $B^2$ | 37738.19 | 1 | 37738.19 | 148.30 | < 0.0001 | ** |
| $AB^2$ | 8041.60 | 1 | 8041.60 | 31.60 | 0.0008 | ** |
| Residual | 1781.28 | 7 | 893.33 | | | |
| Lack of Fit | 72.56 | 3 | 24.19 | 0.0566 | 0.9799 | |
| Pure Error | 1708.72 | 4 | 427.18 | | | |

***Response surface analysis***

The response surface analysis method was employed to analyze the test data, aiming to investigate the intrinsic relationship between the core performance indicators and key influencing factors of the direct injection wing shovel. Based on the data analysis results, response surface plots of each factor with respect to the soil coverage rate were generated. These plots visually illustrate the specific impact of each influencing factor on the performance evaluation index of the direct injection wing shovel, as well as how these factors interact and jointly influence the evaluation index.

Effects of the experimental factors on soil coverage rate

Response surface analysis was used to evaluate the effects of penetration angle, tail-wing depth, and operating speed on the soil coverage rate of the direct-injection winged shovel. The response surface plots shown in Fig. 8 illustrate the effects of pairs of factors and their interactions on soil coverage rate while the third factor is held at its center level. These plots show the direction and magnitude of the factor effects and reveal how their interactions influence soil coverage performance.

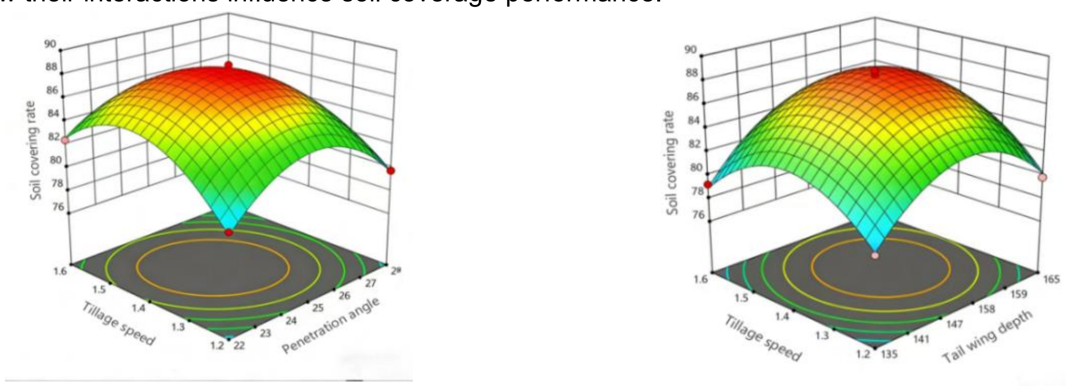


(a) Interaction between penetration angle and tillage speed (b) interaction between tail-wing depth and tillage speed

**Fig. 8 - Effects of factor interactions on the soil coverage rate of the direct-injection winged shovel**

As shown in Fig. 8(a), under the interactive influence of the penetration angle and the tillage speed, as both the tillage speed and the soil penetration angle increase, the soil coverage rate overall exhibits a trend of first increasing and then decreasing.

The magnitudes of change in the soil coverage rate with respect to the increase and decrease of the tillage speed are approximately equal, and the change pattern is relatively uniform. The soil coverage rate reaches its peak when the tillage speed is approximately 1.5 m·s$^{-1}$. The overall response surface is convex.

As can be seen from Fig. 8(b), under the interactive influence of the tillage speed and the tail wing depth, the slope of the tangent plane of the response surface first gradually decreases and then becomes steeper, with the tangent slope also first decreasing and then increasing. The influence trends of the two factors are relatively similar, and the soil coverage rate is more significantly affected by the tail wing depth than by the tillage speed.

The influence on the tillage resistance of the direct injection wing shovel

Response surface methodology was applied to analyze the experimental data, with a comprehensive investigation into the interactive effects of key influencing factors—penetration angle, tail wing depth and tillage speed—on the tillage resistance, a critical performance index of the direct injection wing shovel. Data analysis further enabled the generation of response surface plots illustrating the relationship between each individual factor and tillage resistance, which are presented in Fig.9.


(a) Interaction between penetration angle and operating speed (b) Interaction between tail-wing depth and operating speed

**Fig. 9 - Effects of factor interactions on the tillage resistance of the direct-injection winged shovel**

As shown in Fig. 9(a), under the interactive influence of the penetration angle and the tillage speed, the resistance overall exhibits a trend of first decreasing and then increasing as both the tillage speed and the penetration angle increase. When the tillage speed is approximately 1.5 m·s$^{-1}$, the resistance reaches its minimum value, and the overall response surface is concave.

As can be seen from Fig. 9(b), under the interactive influence of the tillage speed and the tail wing depth, the resistance is significantly more affected by the tail wing depth than by the tillage speed, and this significant influence is completely opposite to the influence on the soil coverage rate.

***Simulation Results for Soil Movement***

As shown in Fig. 10, when the direct-injection winged shovel is fully engaged with the soil, its tip penetrates the plow pan and loosens the compacted soil layer. As the shovel advances, the shovel tip cuts and lifts the soil, causing soil particles to move upward. The winged shovel body then displaces the lifted soil laterally, creating a furrow. After the shovel passes, the displaced soil falls back into the furrow behind the shovel, thereby completing the furrow-opening and soil-covering process.

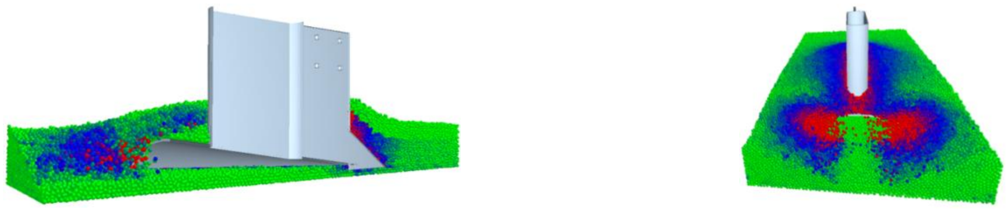

(a) Soil movement at 2.2 seconds

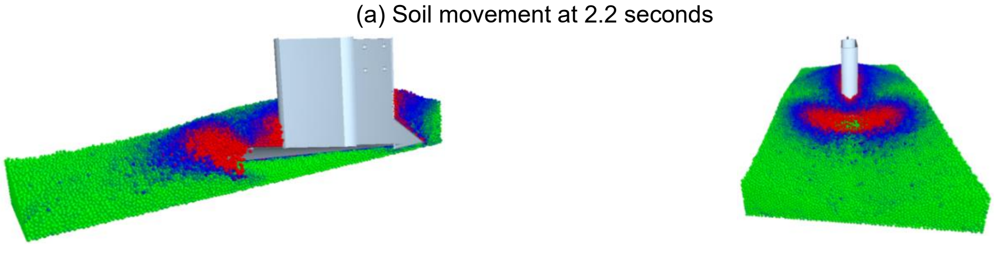

(b) Soil movement at 2.8 seconds

**Fig. 10 - Soil displacement dynamics during operation of direct injection winged shovel**

***Field trial***

Test conditions

The test equipment comprised a deep straw incorporation machine equipped with the direct-injection winged shovel, a draft-force measurement system, measuring tapes, straightedges, marker poles, and sampling shovels. Field tests were conducted after the autumn harvest to evaluate the operational performance of the shovel and validate the simulation results. Before testing, the dimensions of the designated test plots were measured with a tape measure, and their boundaries were marked with poles in accordance with NY/T 500–2002, *Operating Quality of Straw-Returning Machines*. The selected field was continuous and uniform, with a stated length of more than 1,500 m. The test area was divided into a principal test plot and reserve plots. If abnormal conditions invalidated a test in the principal plot, a comparable reserve plot was used. Field topography and soil conditions were considered when selecting the plots to ensure comparable and representative testing conditions.

Performance Test

The performance evaluation of the direct-injection winged shovel focused on its furrow-opening and soil-covering performance. The selected evaluation indicators were furrow-depth stability, furrow-width consistency, and soil coverage rate.

To measure furrow depth, loose soil was carefully removed from the furrow edges and bottom to expose the original soil surface and furrow bottom. A straightedge was placed across the furrow, and the vertical distance from the straightedge to the furrow bottom was measured as the furrow depth. Before measuring furrow width, naturally collapsed soil was removed. Width measurements were taken at longitudinal positions of 0, 150, and 300 mm, and their mean was calculated as the furrow width. The soil coverage rate was determined within a 100 × 300 mm sampling area. The masses of soil displaced outside the furrow and soil that naturally fell back into the furrow were measured separately. The soil coverage rate was calculated as the mass of soil returned to the furrow divided by the total mass of displaced soil.

As shown in Table 6, the mean furrow depths obtained in five consecutive test runs were 305, 302, 301, 298, and 299 mm, respectively. The furrow-depth stability coefficient exceeded 94% in all runs, indicating that the direct-injection winged shovel maintained consistent operating depth across repeated field tests.

**Table 6**

**Field test results for furrow depth**

| Parameters | | First run | Second run | Third run | Fourth run | Fifth run |
|---|---|---|---|---|---|---|
| Furrow depth | Maximum/mm | 308 | 307 | 311 | 306 | 310 |
| | Minimum/mm | 291 | 297 | 286 | 294 | 297 |
| | Average value/mm | 305 | 302 | 301 | 298 | 299 |
| | Range/mm | 17 | 10 | 25 | 12 | 13 |
| | Stability coefficient | 94.75 | 98.34 | 94.17 | 95.48 | 95.32 |

To determine the backfilling rate of the direct injection wing shovel, the furrow depth must first be precisely measured *(Bao et al., 2017; Du et al., 2025).* Specifically, soil accumulated both inside and outside the furrow was thoroughly cleared using shovels to ensure the original ground surface and furrow bottom were fully exposed. Next, a straightedge was placed between the furrow walls to measure the vertical height from the furrow bottom to the ground surface.

As shown in Table 7, the average furrow width of the direct injection wing shovel across five consecutive operations was 1008 mm,1004 mm,1005 mm,1003 mm, and 1009 mm, respectively. The maximum deviation in furrow width during each operation never exceeded 20 mm.

Moreover, the furrow-width consistency coefficient exceeded 95% in all five test runs, indicating that the shovel maintained a consistent furrow width. These results demonstrate stable furrow-opening performance over different operating distances.

**Table 7**

**Field test results for furrow width**

| **Parameters** | | **First run** | **Second run** | **Third run** | **Fourth run** | **Fifth run** |
|---|---|---|---|---|---|---|
| Furrow width | Maximum/mm | 1017 | 1011 | 1014 | 1010 | 1016 |
| | Minimum/mm | 1002 | 995 | 994 | 994 | 998 |
| | Average value/mm | 1008 | 1004 | 1005 | 1003 | 1009 |
| | Range/mm | 15 | 16 | 20 | 16 | 18 |
| | Consistency coefficient | 95.39 | 95.44 | 96.43 | 96.32 | 96.52 |


**Fig. 11 - Operating process of the direct-injection winged shovel during furrow opening and soil covering**

During operation, the shovel tip and body penetrate and lift the soil. The displaced soil moves rearward along the shovel body and subsequently falls into the cavity formed behind the shovel. As shown in Fig.11, this cavity provides space for straw placement. After the straw is guided into the cavity, the displaced soil falls back and covers it, thereby completing the deep straw incorporation process. Field tests confirmed that the direct-injection winged shovel performed its intended functions during deep straw incorporation *(Gao et al., 2022)*.

As shown in Table 8, the mean soil coverage rates recorded in five consecutive test runs were 87.45%, 88.05%, 87.55%, 86.75%, and 87.55%, respectively. The small variation among the five mean values indicates that the shovel maintained relatively consistent soil-covering performance across repeated tests.

**Table 8**

**Experimental results of soil coverage rate**

| Parameters | | First run | Second run | Third run | Fourth run | Fifth run |
|---|---|---|---|---|---|---|
| Soil coverage rate | Maximum/mm | 88.7 | 89.3 | 88.9 | 92.1 | 89.4 |
| | Minimum/mm | 83.5 | 85.5 | 83.2 | 85.4 | 83.7 |
| | Average value/mm | 87.45 | 88.05 | 87.55 | 86.75 | 87.55 |
| | Range/% | 5.2 | 4.7 | 5.7 | 6.5 | 5.7 |

***Experimental Comparative Verification***

As shown in Table 9, the variation patterns of simulation results and field experiment results are largely consistent, with relative errors for both indicators below 3%, indicating high agreement. The minor discrepancies mainly stem from the following factors: the simulation model simplifies soil as a homogeneous medium, neglecting random variables such as straw residues and local moisture fluctuation; additionally, slight systematic errors exist in soil contact parameter calibration, leading to minor deviations between simulation and measured results. Standard deviation and 95% confidence interval analyses demonstrate that field experiment data exhibit low dispersion and good repeatability, confirming that this discrete element model meets the accuracy requirements for simulation analysis.

**Table 9**

| **Evaluating indicator** | **Experimental Mean value** | **Simulation mean** | **Relative error** | **Standard deviation** | **Confidence interval** |
|---|---|---|---|---|---|
| Tillage resistance | 2121.00 | 2063.13 | 2.73 | 24.73 | [2089.81,2152.19] |
| Soil coverage rate | 87.47 | 88.29 | 0.94 | 0.47 | [86.89,88.05] |

## CONCLUSIONS

To address the insufficient operating depth, limited soil-backfilling capability, and high tillage resistance of conventional furrow-opening and soil-covering components, an integrated direct-injection winged shovel was developed. The effects of its structural and operating parameters on soil coverage and tillage resistance were investigated through theoretical analysis, discrete element simulation, and field testing. The main conclusions are as follows:

(1) The soil properties varied with depth. Moisture content ranged from 15.99% to 22.04%, while bulk density increased from 1.41 to 1.54 g/cm³ from the cultivated layer to the subsoil. The shear strength of the plow pan was 30.43 kPa, which was higher than the 23.30 kPa measured in the cultivated layer. These data provided the basis for designing the direct-injection winged shovel and calibrating the soil model.

(2) EDEM simulation results showed that the direct-injection winged shovel effectively disrupted the plow pan and promoted automatic soil backfilling, with a soil coverage rate of 88.45% and a tillage resistance of 2048.78 N, achieving lower energy consumption than traditional two-step operations.

(3) The optimal parameter combination comprised a shovel-tip penetration angle of 25°, a tail-wing depth of 150 mm, and an operating speed of 1.4 m/s. Under these conditions, the predicted soil coverage rate exceeded 88%, while the tillage resistance remained below 2050 N.

(4) Field tests confirmed that the direct-injection winged shovel performed its intended functions during deep straw incorporation. The reported furrow-depth stability, furrow-width consistency, and soil coverage values were 94.65%, 96.06%, and 87.47%, respectively. The measured performance indicators met the requirements of the applicable Chinese agricultural machinery standard, demonstrating stable furrow opening and soil covering under the tested field conditions.

（5）This study has several limitations. In the discrete element model, each soil layer was treated as a homogeneous medium, and field-scale soil heterogeneity, stones, and crop residues were not represented. These simplifications may have contributed to differences between the simulated and measured results. Moreover, the field tests were conducted only in relatively loose black soil in Northeast China. The performance of the shovel in compacted loess, cohesive paddy soil, and sandy loam therefore remains unknown. Hard soil may accelerate component wear, cohesive soil may adhere to the shovel and obstruct straw delivery, and loose sandy soil may not provide stable soil coverage. In addition, the integrated curved tail-wing structure results in a relatively large overall width, potentially limiting maneuverability in narrow-row fields. Future research should optimize the tail-wing profile to reduce the transverse dimensions, conduct comparative tests in different soil types, and develop a DEM model that accounts for spatial soil heterogeneity. These improvements would enhance simulation accuracy and broaden the applicability of the device.

## ACKNOWLEDGEMENT

This research was supported by General Program of Natural Science Foundation of Liaoning Provincial Science and Technology Plan Joint Funds (2025-MSLH-613) and Shenyang Science and Technology Plan Project (24-216-2-10).

## REFERENCES

[1] Awachat, S., & Sharma, D. (2024). A Review on Impact of Agricultural Mechanization on Farm Productivity and Factors Facilitating the Growth of Mechanization, *Institute of Electrical and Electronics Engineers Inc*.pp. 1163–1166. DOI:10.1109/ICDICI62993.2024.10810850.

[2] Aikins, K.A., Barr, J.B., Ucgul, M., Ucgul, M., Jensen, T.A., Antille, D.L., & Desbiolles, J.M. (2020). No-tillage furrow opener performance: A review of tool geometry, settings and interactions with soil and crop residue, *Soil Research*, Vol.58, pp. 603–621. DOI:10.1071/SR19153.

[3] Bao, P., Wu, M., Guan, C., Luo, H., He, Y., & Xiang, W. (2017). Design of plow-rotary style ditching and ridging device for rapeseed seeding (犁旋组合式油菜播种开沟起垄装置设计). *Transactions of the Chinese Society of Agricultural Engineering*, Vol. 33, pp. 23–31. DOI: 10.11975/j.issn.1002-6819.2017.20.003.

[4] Barr, J., Desbiolles, J., Ucgul, M., & Fielke, J. (2020). Bentleg furrow opener performance analysis using the discrete element method. *Biosystems Engineering*, Vol.189, pp.99-115. DOI: 10.1016/j.biosystemseng.2019.11.008.

[5] Cedik, J., Praan, R., Leger, V., Havlicek, M., Lopot, F., Rybansky, M., & Pexa, M. (2024). three-point hitch dynamometer for measuring tractor-implement forces, *Applied Engineering in Agriculture*, Vol. 40, pp. 303–310. DOI: 10.13031/aea.15731.

[6] Du, W., Lin, J., Li, X., Li, L., Zhang, Q., & Liao, Q. (2025). Design and Experiments of the shallow plow for the high-speed strip micro-ridge combined direct seeding machine for rapeseed (油菜高速带状微垄联合播种机浅犁设计与试验). *Transactions of the Chinese Society of Agricultural Engineering*, Vol. 41, pp. 38–48. DOI:10.11975/j.issn.1002-6819.202411157.

[7] Fang, L., Wang, Y., Deng, D., Yuan, S., & Wang, Z. (2021). Research Status and Development Trend Of Mechanized Straw Returning Technology. *INMATEH - Agricultural Engineering*, Vol. 65, pp. 465–475. DOI: 10.35633/inmateh-65-48.

[8] Gao, W.-Y., Lin, J., Li, B., Wang, W., & Gu, S. (2022). Vibration characteristics analysis and structural optimization of straw deep bury and returning machine (秸秆深埋还田机振动特性分析与结构优化). *Transactions of the Journal of Jilin University*, Vol. 52, pp. 970–980. DOI: 10.13229/j.cnki.jdxbgxb20200882.

[9] Jin, F., Liu, D., Zhong, C., Yao, K., Tong, J., & Jiang, Z. (2024). Parameter calibration and discrete element model of highland barley stem based on EDEM. *INMATEH - Agricultural Engineering*, Vol. 72, pp. 363–373. DOI: 10.35633/inmateh-72-33

[10] Liu, G., Wang, K., Chen, X., Gong, J., Deng, Z., & Li, B. (2025). Research on contact parameter calibration and experiment of discrete element simulation model for rice straw. *INMATEH - Agricultural Engineering*, Vol.77, pp. 215–226. DOI: 10.35633/inmateh-77-17

[11] Lin, H., He, J., Li, H., Wang, Q., & Lu, C. (2022). Design and Experiment of a Reciprocating Intermittent Chopping Device for Maize Straw Returning, Agriculture-Basel, Vol.12(2). DOI: 10.3390/agriculture12020220.

[12] Lu, F., Meng, J., & Cheng, B. (2024). How does improving agricultural mechanization affect the green development of agriculture? Evidence from China. *Journal of Cleaner Production*, Vol. 472. DOI: 10.1016/j.jclepro.2024.143298.

[13] Madhusudan, B. S., Kushwaha, H. L., Kumar, A., & Mattar, M. A. (2024). Critical assessment of furrow openers and operational parameters for optimum performance under conservation tillage, Scientific Reports, Vol.14(1). DOI:10.1038/s41598-024-70569-2.

[14] Si, Y., He, M., Chen, S., Liu, Z., Li, Y., Yao, F., & Lu, J (2025). Effects of Deep Plowing and Returning Straw on Corn Yield and Black Soil Fertility under Corn-Soybean Rotation in the Northeast Black Soil Region (东北黑土区玉米-大豆轮作下秸秆深翻还田对玉米产量及黑土肥力的影响). *Transactions of the Corn Science*, Vol. 33(11), pp. 98–105. DOI: 10.13597/j.cnki.maize.science.20251112.

[15] Shen, T., Liu, H., Wu, X., & Sun, X. (2022). Research Status and Prospect of Straw Mechanization and Returning Technology and Equipment（秸秆机械化还田技术及装备研究现状与展望). *Transactions of the Jiangsu Agricultural. DOI:10.15889/j.issn.1002-1302.2022.15.001.*

[16] Wang, R., Li, D., LI, P., Bai, X., Wang, T ., Wang, W., & Zhao, Y. (2023). Optimum design for breaking device with double roller based EDEM. *INMATEH - Agricultural Engineering*, Vol. 70, pp. 570–582. DOI: 10.35633/inmateh-70-55.

[17] Wang, S., Huang, H., Zhang, Y., Yin, C., & Richel, A. (2021). The effect of corn straw return on corn production in Northeast China: An integrated regional evaluation with meta-analysis and system dynamics. Resources, *Conservation and Recycling*, Vol. 167. DOI: 10.1016/j.resconrec.2021.105402.

[18] WEI, L., LI, J., Meng, X., & Li, L. (2025). Design and experiment of subsoiling shovel with offset column and curved surface based on discrete element method (基于离散元法的偏柱式曲面深松铲设计与试验).*Transactions of Shenyang Agricultural University*, vol. 56(5), pp. 135-146. DOI:10.3969/j.issn.1000-1700.2025.05.015

[19] Xu, S.-C., Tao, G., Yi, S., Wang, S., & San, Y. (2025). Design and testing of bionic winged deep-loosening shovel for a strip tillage deep-loosening fertilization machine. *INMATEH - Agricultural Engineering*, Vol.77, pp. 550–562. DOI:10.35633/inmateh-77-45.

[20] Xu, G., Xie, Y., Liang, L., Ding, Q., Xie, H., & Wang, J. (2022). Straw-Soil-Rotary Blade Interaction: Interactive Effects of Multiple Operation Parameters on the Straw Movement, *Agronomy*-Basel, Vol.12(4). DOI:10.3390/agronomy12040847.

[21] Zhang, N., Bai, L., Wei, X., Li, T., Tang, Y., Zeng, X., Lei, Z., Wen, J., & Su, S. (2025). Promoted decomposition in straw return to double-cropped rice fields controls soil acidity, increases soil fertility and improves rice yield. *Chemical Engineering Journal*, Vol. 509. DOI:10.1016/j.cej.2025.161309.